Journal of Fluorine Chemistry 130 (2009) 1086–1092

Contents lists available at ScienceDirect

Journal of Fluorine Chemistry

journal homepage: www.elsevier.com/locate/fluor

# Recent developments in the preparation of high surface area metal fluorides

Tomaž Skapin *, Gašper Tavčar, Andreja Benčan, Zoran Mazej

*Jožef Stefan Institute, Jamova 39, SI-1000 Ljubljana, Slovenia*

ARTICLE INFO

*Article history:*
Received 16 May 2009
Received in revised form 19 June 2009
Accepted 22 June 2009
Available online 1 July 2009

*Keywords:*
Metal fluorides
$AlF_3$
$CrF_3$
High surface area
Nanostructure
TEM

ABSTRACT

An overview of the main procedures for the preparation of fluorides with very high surface areas is given. Three processes are outlined: (i) plasma fluorination, (ii) sol–gel route and (iii) oxidative decomposition of inorganic precursors. From all three processes nanostructured metal fluorides with 100–400 $m^2 g^{-1}$ can be obtained. Prevention of the local overheating during fluorination seems to be the key factor to obtain the high surface area fluorides. TEM investigations of $AlF_3$ and $CrF_3$ obtained by oxidative decomposition revealed considerable differences in their morphologies and crystallinity. $CrF_3$ is completely amorphous and unstable under beam. $AlF_3$ contains an amorphous phase and nanocrystalline phases of α-$AlF_3$ and β-$AlF_3$. Nanocrystals are uniformly distributed within the amorphous phase. Also present are the rod-like nanostructures that consist of β-$AlF_3$ and are 5–10 nm wide.



## 1. Introduction

Use of metal fluorides as catalysts is one of the technically most important applications for these materials. Solid metal fluorides were mainly used as heterogeneous catalysts in fluorination and related processes. For these reactions, aluminium- or chromium-based catalysts were most frequently used [1]. In the last three decades, heterogeneous catalysis on these catalysts played a decisive role in the phase-out of ozone-depleting chlorofluorocarbons (CFCs) [2]. Related catalytic processes included syntheses of hydrochlorofluorocarbons (HCFCs) or hydrofluorocarbons (HFCs) as alternatives for CFCs, environmentally safe destruction of CFCs and conversion of CFCs into environmentally more acceptable products, mainly HFCs.

In classical preparations, solid metal fluorides are usually obtained by fluorination of adequate starting substances with reactive fluorinating agents at elevated temperatures or by thermal decompositions. For thermodynamic reasons, formation of nanostructured fluorides with high surface area is not favoured under such conditions. Typical products are partially or completely crystallised fluorides with surface areas that rarely exceed 50 $m^2 g^{-1}$ with typical values in the range of 10–30 $m^2 g^{-1}$. Classical approach to prepare metal fluorides or fluorinated materials with higher surface areas for catalytic applications is the fluorination of high surface area oxides. Depending on the fluorination conditions and the metal oxide used, the final products may contain considerable amounts of unconverted oxide. Relatively high surface areas that may be found in such materials (>50 $m^2 g^{-1}$) are usually due to the unconverted oxide matrix. In some rare cases materials with surface areas larger than 100 $m^2 g^{-1}$ were prepared, i.e. fluorinated chromia [3–5] and $MgF_2$ [6]. For fluorinated chromia it is clear that the material is not a pure fluoride but a mixture of fluoride and unconverted oxide [4,5].

This overview is focused on pure metal fluorides and related materials. With this restriction in mind, three categories of surface areas can arbitrarily be set: (i) normal (<50 $m^2 g^{-1}$), (ii) intermediate (50–100 $m^2 g^{-1}$) and (iii) high (>100 $m^2 g^{-1}$). Normal surface areas include practically all fluoride materials obtained by conventional preparation procedures. Large majority of metal fluorides falls in this category. Intermediate surface areas are found in materials prepared under specific conditions and/or with specific techniques, like microwave synthesis of $Al(OH,F)_3 \cdot xH_2O$ compounds with interesting acid–base characteristics [7,8]. Fluorides with high surface area, denoted further on as HS fluorides, can be prepared only by very specific procedures, as described in the continuation. Systematic work on these materials started a decade ago.

This contribution gives a brief overview of the progress achieved in the last years in the preparation of HS and nanostructured metal fluorides, i.e. metal fluorides with surface areas higher than 100 $m^2 g^{-1}$ and average particle sizes below 20 nm. Two established preparation procedures, plasma fluorination and non-aqueous sol–gel route, and the newly developed oxidative decomposition are shortly outlined. TEM investigations of HS metal fluorides from oxidative decomposition with some new insights in the nanostructure of these fluorides are also included.

* Corresponding author.
*E-mail address:* tomaz.skapin@ijs.si (T. Skapin).

0022-1139/$ – see front matter © 2009 Elsevier B.V. All rights reserved.
doi:10.1016/j.jfluchem.2009.06.015

## 2. Preparation of high surface area metal fluorides

The present overview of novel procedures for the preparation of HS metal fluorides is limited to the processes that meet the following two criteria: (i) final products are essentially pure metal fluorides or hydroxyfluorides and (ii) surface areas of the final products are higher than the arbitrary set limit of 100 $m^2 g^{-1}$. It should be noted that fluorides with such characteristics usually differ markedly from the corresponding bulk crystalline fluorides which have practically the same chemical composition but much lower surface areas.

Procedures for the preparation of bulk HS metal fluorides and the corresponding HS metal fluoride products are summarised in Table 1. Three different synthetic approaches are currently available: (i) plasma fluorination, (ii) sol–gel procedure and (iii) oxidative decomposition. Among these three, sol–gel procedure was most extensively investigated due to its versatility. On the other side, plasma fluorination and oxidative decomposition represent an inorganic alternative to the sol–gel process and enable the preparation of complementary HS fluorides that are not contaminated with carbon residues. In addition, oxidative decomposition is apparently the only approach that currently allows the preparation of HS-$CrF_3$. Majority of the work was done on $AlF_3$ that, according to calculations for free gaseous molecules [19], closely approaches the acidity of the strongest Lewis acid, $SbF_5$. Search for highly Lewis acidic solid materials with possible unprecedented functionalities was the main impetus for intense investigations of the HS-$AlF_3$ materials performed in the last 5 years.

### 2.1. Plasma fluorination

One of the first reports on the synthesis of bulk HS metal fluorides appeared in 2001 when the preparation of $AlF_3$ with 190 $m^2 g^{-1}$ was reported [9]. This HS fluoride was obtained by plasma fluorination of silica-rich zeolite, $H_{1.3}[Al_{1.3}Si_{22.7}O_{48}]$ (zeolite H-SSZ-32), performed below 180 °C with $NF_3$ as the fluorinating agent. Similar fluorination of different aluminium oxide precursors yielded products with surface areas of 6–15 $m^2 g^{-1}$ that consisted of unconverted oxide and α-$AlF_3$, while the fluorination of aluminium silicate with lower silica content, $Al_2Si_2O_5(OH)_4$ (kaolinite), resulted in a product consisting of α-$AlF_3$ and β-$AlF_3$ with surface area of 32 $m^2 g^{-1}$. Formation of the HS-$AlF_3$ product was attributed to the low spatial density of Al atoms in the silica-rich zeolite precursor and to the fluorination under "cold" plasma conditions. Combination of both effects was crucial in preventing the thermally induced ordering and crystallisation of the fluoride phase that remained nearly amorphous with a highly distorted arrangement of $AlF_6$ octahedra. Thermal stability of the amorphous plasma-derived $AlF_3$ was investigated recently by temperature-programmed synchrotron X-ray powder diffraction [20]. Amorphous $AlF_3$ was found to be stable up to 330 °C, at higher temperatures it was converted first to β-$AlF_3$ and above 440 °C to cubic-$AlF_3$, the high-temperature modification of α-$AlF_3$. For other $AlF_3$ materials, either derived from different precursors or prepared in different ways, substantial shifts from the above values could be observed. These divergences were attributed to the presence of different residual by-products that can either accelerate or retard the transformation processes. Some of the unusual features of HS-$AlF_3$ materials, like the very high acidity and the related catalytic activity, are often correlated with a high degree of structural disorder found prevalently in the amorphous $AlF_3$ phase.

### 2.2. Non-aqueous sol–gel route

Sol–gel procedure, firstly reported in 2003 by Kemnitz et al. [10], is currently the core methodology for the preparation of a variety of HS metal fluorides. Sol–gel procedure, originally developed for the synthesis of HS-$AlF_3$, was later adopted for the preparation of a number of binary and complex metal fluorides as well as mixed and doped fluorides. Details about the preparation procedure, underlying chemistry, properties of the HS fluorides obtained and an outlook on their possible applications can be found in a comprehensive review of the sol–gel synthesis of nanostructured metal fluorides that was published recently [11]. Only a general overview of the sol–gel process, mainly in relation with the HS-$AlF_3$ preparation, is given here. Also included are some of the most recent achievements related to the sol–gel process that appeared after the above mentioned review.

Main fluorination of the starting substances, prevalently metal alkoxides dissolved in non-aqueous solvents, is performed at room temperature with anhydrous hydrogen fluoride (aHF) dissolved in alcohol or diethyl ether. The sol–gel approach to HS metal fluorides can therefore be categorised as a typical chimie douce (soft chemistry) process. In the formed fluoride gels some of the binding

**Table 1**
Overview of the preparation procedures to HS metal fluorides.

| Metal fluoride | Procedure | Fluorination | | Product[a] | | References |
|---|---|---|---|---|---|---|
| | | Precursor | F source/temperature (°C) | BET surface area ($m^2 g^{-1}$) | Phases; composition | |
| $AlF_3$ | Plasma | $H_{1.3}[Al_{1.3}Si_{22.7}O_{48}]$ (zeolite H-SSZ-32) | $NF_3$ plasma/180 | 190 | Amorphous (α-$AlF_3$ and β-$AlF_3$) | [9] |
| $AlF_3$ | Sol–gel | Al-alkoxides | HF[b]/25<br>HF, CFC, HCFC/100-350 | 200–420 | Amorphous; F/Al ~ 3 | [10,11,12] |
| $AlF_3$ | Oxidative decomposition | $N_2H_6AlF_5$ | $F_2$/25; in liquid aHF | 180–280 | Amorphous (nano α-$AlF_3$ and β-$AlF_3$); F/Al = 2.94–3.17 | [13] |
| $AlF_3$ | Sol–gel | Al-isopropoxide | HF[b]/25 + 180 (microwave) $F_2$/220 | 330 | α-$AlF_3$ + unknown | [14] |
| $Al(F,OH)_3$ | Sol–gel | Al-isopropoxide | HF + $H_2O$[b]/25 | 215–502 | F/Al = 1–2.6 | [15] |
| $CrF_3$ | Oxidative decomposition | $N_2H_6CrF_5{\cdot}H_2O$ | $F_2$/25; in liquid aHF | 200–300 | Amorphous; F/Cr = 3 | [16] |
| $MgF_2$ | Sol–gel | Mg-methoxide | HF[b]/25 | 150–350 | Amorphous | [11] |
| $Mg(F,OH)_2$ | Sol–gel | Mg-methoxide | HF + $H_2O$[b]/25 | 180–424 | F/Mg = 1.9–2.1 | [17] |
| $MgF_2$ + MgO | Sol–gel | Mg-methoxide | HF + $H_2O$/25 | 100–450 | Mixtures of $MgF_2$ and MgO | [18] |
| $CaF_2$ | Sol–gel | Ca-methoxide-ethoxide | HF[b]/25 | 324 | Amorphous ($CaF_2$) | [11] |

[a] Amorphous products usually show very broad reflections from which the exact fluoride phase(s) cannot be unambiguously identified.
[b] In sol–gel preparations: HF or HF + $H_2O$ dissolved in organic solvent (alcohol, diethyl ether).

sites are occupied by organic groups that prevent the crystallisation of the fluoride phase. Consequently, fluorides remain structurally highly disordered, amorphous to X-rays and have very high surface areas. For example, dried gels of the highly acidic $AlF_3$ have extremely high surface areas that may exceed 500 $m^2 g^{-1}$ and contain a considerable amount of organic residue that, expressed as carbon content, may exceed 30 wt.%. Another characteristic of the dried $AlF_3$ gels is that they do not show catalytic activity in model Lewis acid catalysed reactions. Catalytic inactivity is associated with blocking of surface active sites with the residual organic species. To attain a catalytically active material, organic residue has to be removed by additional fluorination performed under gas–solid conditions at intermediate temperatures. This step showed to be decisive in obtaining highly Lewis acidic and catalytically active HS-$AlF_3$ [12]. To achieve these characteristics with good repeatability and to prevent crystallisation with excessive drop of surface area, fluorination parameters must be well balanced and fully optimised. Key preparation parameters were therefore thoroughly investigated [12]. Various fluorocarbons (CFCs, HFCs or HCFCs) or HF were used as gaseous fluorinating agents [11,12]. HS-$AlF_3$ materials with best characteristics were usually obtained when compounds with lower hydrogen content, like $CCl_2F_2$ or $CHClF_2$, were used as fluorinating agents. Typical HS-$AlF_3$ obtained under optimal preparation conditions has 250 $m^2 g^{-1}$, contains 0.3% of residual carbon and is active in 1,2-dibromoheksafluoropropane (1,2-DBP) isomerisation to 2,2-dibromoheksafluoropropane [12]. It should be noted that this isomerisation proceeds only in the presence of very strong Lewis acids, like aluminium chlorofluoride (ACF) or antimony pentafluoride, $SbF_5$. Attempts to remove the remaining carbon impurities from a typical HS-$AlF_3$ by additional fluorination with elemental fluorine, $F_2$, at 130 or 200 °C resulted in HS materials with lower surface areas that were inactive in 1,2-DBP isomerisation [12]. These effects were correlated with the thermally induced reorganisations in $AlF_3$ due to the strongly exothermic reaction with $F_2$. On the other side and rather surprisingly, direct fluorination with $F_2$ at 225 °C of dried $AlF_3$ gel with 12 wt.% of carbon and 525 $m^2 g^{-1}$ yielded a partially crystallised HS-$AlF_3$ with 330 $m^2 g^{-1}$ that was active in 1,2-DBP isomerisation [14].

In the past 5 years the sol–gel process has evolved into a versatile tool for the preparation of a broad range of HS fluoride materials. Another asset of this process is that it allows, within reasonable limits, a quite accurate tailoring of some properties. In a recent work, the original sol–gel procedure was combined with a microwave solvothermal process that resulted in the formation of partially crystallised $AlF_3$ products with relatively very high surface areas that were largely retained also after fluorination with $F_2$ at medium temperatures, as mentioned above [14]. Sol–gel procedure, at the beginning prevalently used for the preparation of pure fluorides, was recently employed also for the preparation of aluminium [15] or magnesium [17] hydroxyfluorides and $MgF_2$/MgO mixtures [18] with outstanding surface areas in the range 180–500 $m^2 g^{-1}$. This was achieved by replacing aHF with hydrofluoric acid in the gel formation step. An important recent achievement was also the use of Lewis and Brønsted acidic magnesium hydroxyfluorides as catalysts in the synthesis of (all-*rac*)-[α]-tocopherol [17]. This synthesis is a rare example of application of fluoride-based catalysts in reactions that do not involve fluorine compounds.

### 2.3. Oxidative decomposition

Oxidative decomposition, as a possible alternative route to HS metal fluorides, is currently investigated in our laboratory. Based on the previous work on hydrazinium fluorometalates [21,22] these compounds were selected as suitable starting substances. Thermal decomposition of hydrazinium fluorometalates is a known route for the preparation of binary fluorides. However, relatively high temperatures, required to complete the decomposition, are not favourable for the preparation of materials with high surface areas. Another approach, decomposition of hydrazinium fluorometalates at room temperature by the reaction with a strong oxidiser, $F_2$, was therefore developed.

New approach to HS metal fluorides was first tested in the oxidative decomposition of hydrazinium(+2) fluoroaluminate, $N_2H_6AlF_5$, with $F_2$ [13]. Under ideal conditions, decomposition of the hydrazinium precursor should yield $AlF_3$ as the only solid nonvolatile product, according to reaction (1).

$$N_2H_6AlF_5 + 2F_2 \rightarrow AlF_3 + N_2 + 6HF \quad (1)$$

Reaction between a strong reducing agent, hydrazinium(+2) ion, $N_2H_6^{2+}$, and a strong oxidiser, $F_2$, is strongly exothermic and can proceed uncontrollably with considerable local overheating of the products. This may lead to the formation of crystalline fluoride with low surface area and, in the case of $AlF_3$, to the formation of catalytically inactive high temperature phase, α-$AlF_3$. The decomposition reaction was therefore studied under two regimes, (i) under heterogeneous (gas–solid) conditions and (ii) in liquid aHF medium. $AlF_3$ products from both procedures show distinctive differences, as seen from the comparison given in Table 2. Surface areas of the $AlF_3$ products from gas–solid reactions were comparable to similar fluorides prepared by conventional methods. Although the control of the gas–solid reaction proved to be very difficult, the repeatability could be improved to some extent with the proper optimisation of some preparation parameters, like by spreading the solid reactant in uniform layers. On the other side, much better control over the decomposition could be achieved when the reaction was carried out in liquid aHF medium. By using the later approach, HS-$AlF_3$ with surface areas up to 300 $m^2 g^{-1}$ were obtained.

Clear differences in morphologies of $AlF_3$ products from both procedures can be observed in SEM micrographs shown in Fig. 1. Decomposition products obtained by gas–solid reaction consist of large agglomerates of irregularly shaped particles (Fig. 1A-left). In addition to irregular particles, a closer inspection reveals the presence of interlaced rod-like crystallites that are approximately 0.1 μm wide and up to 1 μm long (Fig. 1A-right). Observed formation of micro crystallites with such dimensions is consistent with powder X-ray diffraction that shows the formation of crystalline α-$AlF_3$ and β-$AlF_3$, as well as with BET data that indicate the formation of particles with average diameter of 0.08 μm (Table 2). Decomposition products obtained in liquid aHF have a different morphology, as shown in Fig. 1B. Irregular particles in the range from 0.5 to several μm show an apparent

**Table 2**
Some properties of the products from oxidative decomposition of $N_2H_6AlF_5$ with $F_2$ under gas–solid conditions or in liquid aHF medium.

| Procedure | Gas–solid reaction | In liquid aHF |
|---|---|---|
| Atom ratio (F/Al) | ~3.0 | 2.95–3.10 |
| X-ray detected phases | α-$AlF_3$, β-$AlF_3$ | Amorphous |
| BET ($m^2 g^{-1}$): | | |
| Obtained range | 5–90 | 130–300 |
| Typical values | 24 ± 3 | 270 ± 20 |
| Average particle diameter[a] (nm) | 83 | 7 |
| Maximum batch (g) | 1 | 10 |
| Catalytic activity in $CClF_2CCl_2F$ isomerisation | No | Yes[b] |

[a] Estimated from BET surface area, assumptions: spherical geometry, non-porous particles, average $AlF_3$ crystal density 3.0 g $cm^{-3}$.
[b] Depending on the $NH_4^+$ content.

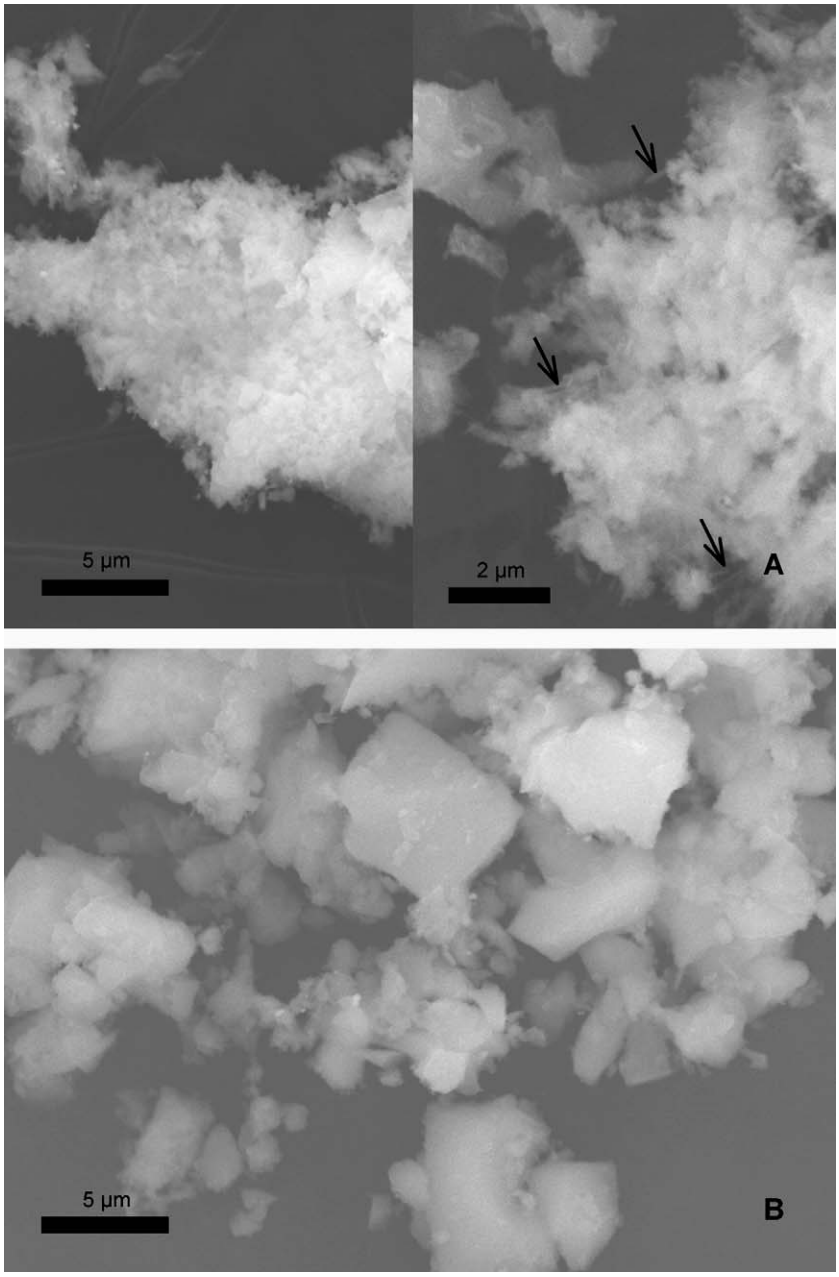


**Fig. 1.** SEM images of products after the decomposition of $N_2H_6AlF_5$ with $F_2$; decomposition was performed under gas–solid conditions (A) or in liquid aHF medium (B). Arrows in A indicate the presence of rod-like 0.1 μm wide crystallites.

homogeneous structure with apparently no crystallisation. Very high surface areas of 200–300 $m^2\,g^{-1}$ and amorphous nature of these materials (Table 2) suggest that the observed micro-sized particles must be porous and composed of much smaller building blocks. This was confirmed by TEM investigations presented further on.

Following the successful preparation of HS-$AlF_3$ by oxidative decomposition in liquid aHF, the same approach was employed for the decomposition of hydrazinium(+2) fluorochromate monohydrate, $N_2H_6CrF_5{\cdot}H_2O$, according to reaction (2) [16].

$$2N_2H_6CrF_5{\cdot}H_2O + 6F_2 \rightarrow 2CrF_3 + 2N_2 + O_2 + 16HF \quad (2)$$

Decomposition is however more complex as shown by reaction (2) and includes also a partial oxidation of $Cr^{3+}$ to $Cr^{>3+}$ and formation of Cr-oxofluorides, mainly in the form of a volatile chromium dioxide difluoride, $CrO_2F_2$. Final decomposition products are therefore relatively pure amorphous $CrF_3$ with very high surface areas ranging from 200 to 300 $m^2\,g^{-1}$. SEM investigations (not shown) indicate that the morphology of HS-$CrF_3$ resembles very much the morphology of HS-$AlF_3$ shown in Fig. 1B.

Oxidative decomposition of hydrazinium precursors containing gallium and iron gave materials with much lower surface areas in the range from 12 to 33 $m^2\,g^{-1}$. Oxidative decomposition of magnesium nitrate hydrate, $Mg(NO_3)_2{\cdot}2H_2O$, with $F_2$ in liquid aHF resulted in a partially crystallised magnesium fluoride, $MgF_2$, with medium range surface area of 70 $m^2\,g^{-1}$.

HS-$AlF_3$ and HS-$CrF_3$ obtained by oxidative decomposition show distinctive Lewis acidity as demonstrated by classical pyridine adsorption tests shown in Fig. 2. Pyridine adsorption on $MgF_2$ derived from the nitrate was much lower, but still detectable, indicating the presence of some Lewis acidity. Position

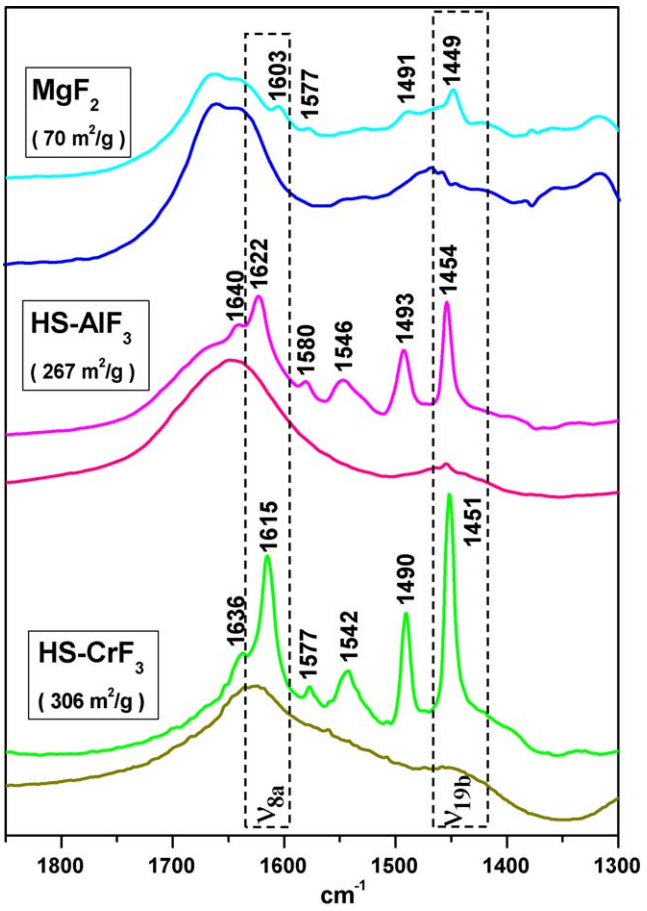


**Fig. 2.** FTIR spectra of metal fluoride products obtained by oxidative decomposition with $F_2$ in liquid aHF and evacuated at 250 °C (upper traces) after pyridine adsorption at 150 °C.

of typical bands, $\nu_{8a}$ and $\nu_{19b}$ modes, associated with pyridine adsorbed on Lewis acid sites shows that the strength of acid sites increases in the expected order: $MgF_2$ < HS-$CrF_3$ < HS-$AlF_3$. Much higher band intensities observed for HS-$AlF_3$ and HS-$CrF_3$ are due to the high surface areas of these materials. In a recent study it was clearly demonstrated that the concentration of Lewis acid sites per gram of material increases with increasing surface area [14]. HS-$AlF_3$ and HS-$CrF_3$ were further investigated in model catalytic reaction with $CCl_2FCClF_2$. General catalytic behaviour exhibited by both HS fluorides is typical for Al- or Cr-based catalysts [1,4], i.e. on highly Lewis acidic HS-$AlF_3$ isomerisation of $CCl_2FCClF_2$ to $CCl_3CF_3$ prevails, while on HS-$CrF_3$ halogen exchange and isomerisation take place simultaneously. Comparison with catalysts investigated earlier [4,5] indicates that both HS fluorides show higher catalytic activity.

## 3. Nanostructure of HS metal fluorides

Nanoaspects of metal fluorides have received considerable attention in the last years. Two reviews dealing with this topic appeared recently [11,23]. Review [23] gives a very broad coverage of the subject with a considerable portion devoted to various processes for the preparation of nano-sized fluorides in the pure form, as one- or two-dimensional nano-objects, or as fluoride nanocomposites. In this review, the upper limit of the nanoregion is set to 100 nm. This limit roughly corresponds to uniformly nanostructured fluorides with surface areas from 10 to 30 $m^2\,g^{-1}$. For the catalytically most relevant fluoride, $AlF_3$, with average crystal density of 3.0 g $cm^{-3}$ the corresponding border area equals 20 $m^2\,g^{-1}$. As mentioned in Section 1, typical fluoride catalysts prepared by conventional methods have surface areas in the range from 10 to 50 $m^2\,g^{-1}$. By accepting the above limit, all these materials fit within the nanostructured fluorides, although as border cases. Second review [11] is focused on the sol–gel route to HS and nano-sized fluorides. Overview of HS fluorides given in Table 1 shows that the surface areas of these materials fall in the range from 100 to 500 $m^2\,g^{-1}$. For $AlF_3$ these areas correspond to particles ranging from 4 to 20 nm; the typical HS-$AlF_3$ with 250 $m^2\,g^{-1}$ consists therefore of 8 nm particles. Considering the simplifications made in the evaluation, it is clear that the basic dimensions found in real HS materials may scatter considerably with some of the particles being much smaller than the values indicated above. Unique features exhibited by HS metal fluorides, and usually not found in conventionally prepared fluorides, can therefore be ascribed to the bulk nanostructure of HS materials in the range well below 20 nm. Comparison of low and high surface areas $AlF_3$ products from oxidative decomposition runs, given in Table 2, gives a good example of how a 10-fold reduction in particle size can affect some of the key characteristics of these materials, like surface area, crystallinity, acidity and related catalytic activity.

### 3.1. TEM investigations of HS fluorides from oxidative decomposition

A common problem with HS metal fluorides when examined by conventional powder X-ray diffraction (XRD) is that they usually show very broad and weak diffraction lines from which it is impossible to unequivocally identify the phases present. Materials are described as amorphous or nearly amorphous [10,20], although the diffuse diffraction lines indicate that a low level of ordering may already be present. The nature, the degree of crystallisation, and morphology of the HS metal fluorides obtained by oxidative decomposition were studied by transmission electron microscopy (TEM, JEM 2100 microscope). Since the samples were highly hygroscopic, as pointed out later, special attention was focused on the preparation of samples for TEM investigations, i.e. the powders were placed on the Ni–C grid in a dry-box and the exposure to ambient air during the transfer into the microscope was kept at the minimum. In addition, samples proved to be extremely beam-sensitive, especially the HS-$CrF_3$ materials that crystallised after prolonged irradiation. All investigations were done using the smallest condenser aperture and spot size. Experimental selected-area electron diffraction (SAED) patterns were compared to calculated (simulated) patterns in order to identify the crystal structure of the phases [24]. Simulated electron diffraction powder patterns were calculated using the Electron Microscopy Image Simulation Package (EMS) program package [25].

As shown in Fig. 3, the microstructure of HS-$AlF_3$ from oxidative decomposition consists of a matrix phase, where beside an amorphous phase, fine crystallites with particle size of 3 nm are found. Corresponding interplanar distances are in the range of 0.34–0.36 nm. Similar range of interplanar distances, 0.34–0.37 nm, was found in previous investigations and assigned generally as $AlF_3$ phases [10,14,15]. Nanocrystallites in current HS-$AlF_3$ materials are uniformly distributed within the surrounding amorphous phase. In order to identify the nanocrystalline phase the experimental SAED patterns were compared to simulated ones for various phases that could be possibly present in the sample, i.e. α-$AlF_3$, β-$AlF_3$, $AlF_3{\cdot}3H_2O$ and $NH_4AlF_4$. In the experimental SAED pattern uniform, slightly diffused circles indicate the presence of very small particles. The experimental pattern can be indexed with the combination of α-$AlF_3$ (ICSD 68826) and β-$AlF_3$ (ICSD 202681) with a particle size around 5 nm (see upper inset in Fig. 3). No match was obtained for $AlF_3{\cdot}3H_2O$ and $NH_4AlF_4$ phases. The Fast Fourier Transform (FFT) performed on the marked region in Fig. 3 additionally confirmed the presence

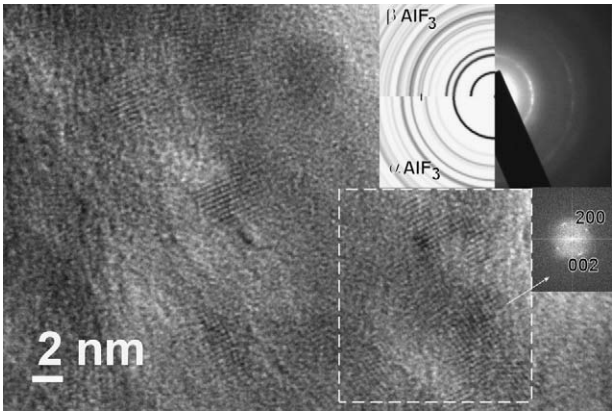


**Fig. 3.** TEM micrograph (bright-field) of around 3 nm sized crystallites embedded in the amorphous phase in HS-$AlF_3$ sample. Upper inset: comparison between the experimental (right) and calculated (left) patterns for α-$AlF_3$ and β-$AlF_3$. In the experimental SAED pattern circles can be matched with the combination of α-$AlF_3$ and β-$AlF_3$ phases. Lower inset: FFT of the marked region. Spots could be indexed as 0 0 2 and 2 0 0 planes of the β-$AlF_3$ phase.

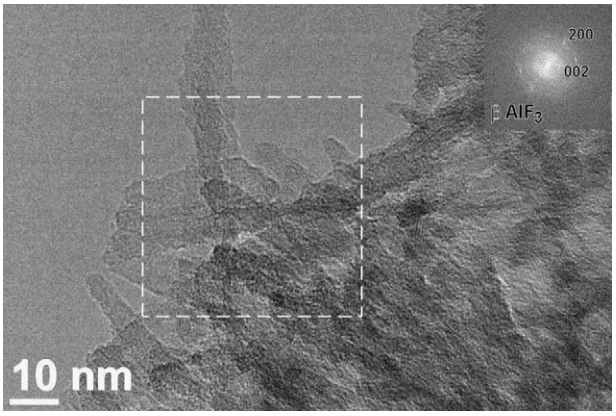


**Fig. 4.** TEM micrograph (bright-field) of nano-rods in HS-$AlF_3$ sample. Inset is FFT of the marked region. Spots could be indexed as 0 0 2 and 2 0 0 planes of β-$AlF_3$.

of β-$AlF_3$ phase in the sample. The spots could be indexed as 0 0 2 and 2 0 0 planes of β-$AlF_3$. Our results clearly confirm the formation of specific nanocrystalline $AlF_3$ phases.

In the same sample the presence of a phase in the form of interlaced arrangement of irregular elongated particles was found, as shown in Fig. 4. These "nano-rods" are 5–10 nm wide. These dimensions are in good agreement with the average particle diameter of 7 nm calculated from the BET data. Using FFT it was determined that this phase is most probably β-$AlF_3$ (Fig. 4). Based on the TEM results we can conclude that the HS-$AlF_3$ sample consists of the matrix phase composed from nanocrystalline α-$AlF_3$ and β-$AlF_3$ and nano-rods consisting of β-$AlF_3$. HS-$AlF_3$ materials from other preparations show slightly different nanostructures: sol–gel derived products usually consist of rounded 10 nm particles [10] or a mixture of 10 and 50 nm particles [14], in the plasma-derived products two types of particles were found, relatively uniform nano-rods 20–50 nm in length and 3–5 nm agglomerated particles [20]. Formation of nano-rods in the later process was tentatively attributed to either anisotropic etching effects found in plasma or to the formation of crystalline hydrate. Namely, plasma-derived HS-$AlF_3$ was found to be very sensitive to moisture, after exposure to air for some days it was converted to a mixture of α-$AlF_3$ and β-$AlF_3{\cdot}3H_2O$ [20]. During our work, formation of crystalline hydrate after longer exposures of HS-$AlF_3$ to ambient air was also observed, but in our case only β-$AlF_3{\cdot}3H_2O$ was formed. Behaviour towards water of both HS-$AlF_3$ products, derived either from plasma or decomposition, is therefore similar. However, rod-like particles found in our HS-$AlF_3$ (Fig. 4) cannot be ascribed to hydrate formation. Under the operation conditions used here excessive hydration of the material was very unlikely. In addition, TEM investigations clearly indicate that the rod-like particles consist of nanocrystalline β-$AlF_3$ (Fig. 4) and we could not detect any $AlF_3{\cdot}3H_2O$ phases.

From the data accumulated so far it is clear that all HS-$AlF_3$ materials exhibit some nanocrystallinity in the range 3–10 nm, irrespective of the very different routes used for their preparation. Crystallinity at this level is usually poorly detected by XRD but can be adequately determined by TEM techniques, as demonstrated here. It is interesting to note that the smallest crystallites or ordered regions detected by TEM, 2–4 nm as shown in Fig. 3, approach closely the length scale of 1.7–2.8 nm for the $6 \times 6 \times 6$ and $8 \times 8 \times 8$ cubic unit cells used in computer modelling to probe the finite size effects and surface properties in α-$AlF_3$ nanoparticles [26]. Based on these simulations the authors concluded that nanosized α-$AlF_3$, due to significant structural rearrangements at the edges and corners, can exhibit considerable Lewis acidity usually not found in larger α-$AlF_3$ crystals. However, in a recent study a different morphology of α-$AlF_3$, calculated from the lowest energy surfaces, was proposed [27]. In this study Lewis acidity of α-$AlF_3$ was found to be much weaker than that predicted for β-$AlF_3$ [28,29]. According to calculations of $NH_3$ binding energies, the strongest Lewis acidic sites on $AlF_3$ surfaces correspond to Al ions fivefold coordinated to bidentate F ions in truncated octahedra [27]. Only a small number of these very strong Lewis acid sites may be present on β-$AlF_3$ while there are no such sites on α-$AlF_3$ crystallites. These findings are in good agreement with experimentally determined activities in Lewis acid catalysed reactions; α-$AlF_3$ is usually completely inactive while the β-$AlF_3$ is an active catalyst in reactions that require moderate Lewis acidity. According to these studies it is clear that crystalline or ordered $AlF_3$ structures cannot exhibit the very strong Lewis acidity found in HS-$AlF_3$ materials from any origin. Very strong acidity in these materials is usually ascribed to the structurally highly disordered amorphous phase that, due to the absence of regularity in the structure, cannot be modelled by current computational methods. Disregarding the possible discrepancies between the above findings it is clear that the extraordinarily high Lewis acidity of HS-$AlF_3$ originates primarily from the structural disorder that is the highest in the amorphous phase. Determining the stability limits of the amorphous phase is therefore crucial for a possible exploitation of these materials.

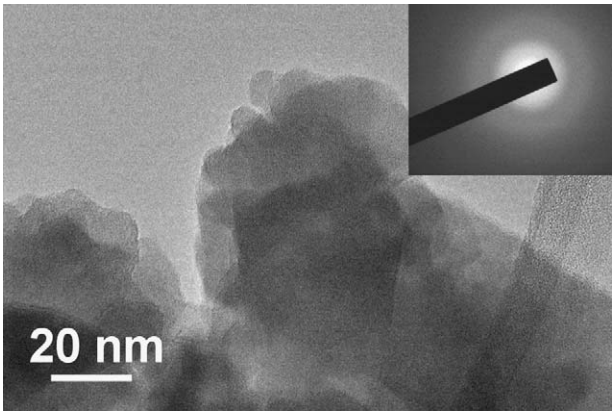


**Fig. 5.** TEM micrograph (bright-field) of HS-$CrF_3$ sample. Inset shows the experimental SAED pattern corresponding to an amorphous phase.

A TEM micrograph and corresponding SAED pattern of the HS-$CrF_3$ sample is shown in Fig. 5. The sample is composed of agglomerated rounded particles with the size down to 10 nm. Due to the extreme beam-sensitivity of this material more detailed TEM investigations were not possible. However, diffuse circles in the experimental SAED pattern indicate that the sample is completely amorphous also in the nanoregion, unlike HS-$AlF_3$ that is partially nanocrystalline. The amorphous nature of HS-$CrF_3$ may have some important implications for its application.

## 4. Conclusions

Three preparative approaches, presented here, allow the preparation of HS metal fluorides with unprecedented characteristics, i.e. surface areas in the range 200–400 $m^2\ g^{-1}$ and Lewis acidities that are comparable to the acidity of the strongest Lewis acid known, $SbF_5$. In addition, the HS fluorides are nanostructured with the dimensions of the basic particles usually below 20 nm. In all three procedures, the basic reaction is fluorination. In contrast to classical fluorination procedures, fluorination to HS fluorides is performed at relatively mild conditions, i.e. at room temperature in the sol–gel and decomposition process or below 180 °C under cold plasma conditions in the plasma process. Efficient prevention of the local overheating during fluorination seems to be the key factor in obtaining the HS fluorides. At low temperatures, processes such as ordering, sintering and crystallisation are considerably slowed down or even stopped that largely preserves the disordered structure found in HS fluorides. All three preparation procedures complement each other and allow the preparation of materials with similar basic characteristics. A common problem of these materials is that due to very high surface areas and amorphous structure they can bind or incorporate considerable amounts of contaminants. Nature of the contaminant depends on the preparation route, i.e. sol–gel derived HS fluorides may contain considerable amounts of organic residues while $NH_4^+$ species may be present in the products from oxidative decomposition. As pointed out earlier, different residual by-products can considerably influence the phase transformation processes in HS-$AlF_3$ [20]. Investigation of HS fluorides from different preparations, containing therefore different residual species, can help to clarify the main processes that influence the stability of HS fluorides what may have important implications for their application.

TEM proved to be a powerful tool to investigate the morphology and crystallinity of nanostructured HS fluorides. TEM investigations of the two oxidative decomposition products, HS-$AlF_3$ and HS-$CrF_3$, have confirmed that these materials are nanostructured and differ in their crystallinity. HS-$CrF_3$ is composed of agglomerates of 10 nm spherical particles and is completely amorphous. HS-$AlF_3$ contains an amorphous phase and a crystalline phase with crystallites in the range 3–10 nm. These nanocrystallites could clearly be identified as α-$AlF_3$ and β-$AlF_3$. Nanocrystallites are uniformly distributed within the amorphous matrix. Larger rod-like nanostructures are 5–10 nm wide and consist of β-$AlF_3$. HS-$AlF_3$ can therefore be considered as a nanocrystalline material. Uniform distribution of crystallites within the grains suggests that the nanocrystalline phase was formed during the oxidative decomposition. It is possible that nanocrystals were formed due to slight local overheating that could not be completely prevented by the liquid aHF medium. Further optimisation of the decomposition process could possibly reduce the amount of crystalline phase in HS-$AlF_3$.

## Acknowledgements

We thank the European Union for funding the FUNFLUOS project (Contract no. NMP3-CT-2004-505575) and the Slovenian Research Agency for funding the research programme P1-0045.

## Appendix A. Supplementary data

Supplementary data associated with this article can be found, in the online version, at doi:10.1016/j.jfluchem.2009.06.015.

## References

[1] E. Kemnitz, J.M. Winfield, in: T. Nakajima, B. Žemva, A. Tressaud (Eds.), Advanced Inorganic Fluorides: Synthesis, Characterization and Application, Elsevier Science S.A., Laussane, 2000, pp. 367–401.
[2] L.E. Manzer, M.J. Nappa, Appl. Catal. A 221 (2001) 267–274.
[3] H.-D. Quan, H.-E. Yang, M. Tamura, A. Sekiya, J. Catal. 231 (2005) 254–257.
[4] H. Bozorgzadeh, E. Kemnitz, M. Nickkho-Amiry, T. Skapin, J.M. Winfield, J. Fluorine Chem. 110 (2001) 181–189.
[5] H. Bozorgzadeh, E. Kemnitz, M. Nickkho-Amiry, T. Skapin, J.M. Winfield, J. Fluorine Chem. 121 (2003) 83–92.
[6] D.H. Cho, Y.G. Kim, M.J. Chung, J.S. Chung, Appl. Catal. B 18 (1998) 251–261.
[7] D. Dambournet, A. Demourgues, C. Martineau, S. Pechev, J. Lhoste, J. Majimel, A. Vimont, J.-C. Lavalley, C. Legein, J.-Y. Buzare, F. Fayon, A. Tressaud, Chem. Mater. 20 (2008) 1459–1469.
[8] D. Dambournet, H. Leclerc, A. Vimont, J.-C. Lavalley, M. Nickkho-Amiry, M. Daturi, J.M. Winfield, Phys. Chem. Chem. Phys. 11 (2009) 1369–1379.
[9] J.L. Delattre, P.J. Chupas, C.P. Grey, A.M. Stacy, J. Am. Chem. Soc. 123 (2001) 5364–5365.
[10] E. Kemnitz, U. Groß, S. Rüdiger, C.S. Shekar, Angew. Chem. Int. Ed. 42 (2003) 4251–4254.
[11] S. Rüdiger, U. Groß, E. Kemnitz, J. Fluorine Chem. 128 (2007) 353–368.
[12] S. Rüdiger, G. Eltanany, U. Groß, E. Kemnitz, J. Sol–Gel Sci. Technol. 41 (2007) 299–311.
[13] Z. Mazej, A. Jesih, B. Žemva, T. Skapin, J.M. Winfield, N. Weiher, A. Makarowicz, S.L.M. Schroeder, unpublished results.
[14] D. Dambournet, G. Eltanamy, A. Vimont, J.-C. Lavalley, J.-M. Goupil, A. Demourgues, E. Durand, J. Majimel, S. Rudiger, E. Kemnitz, J.M. Winfield, A. Tressaud, Chem. Eur. J. 14 (2008) 6205–6212.
[15] C. Stosiek, G. Scholz, G. Eltanany, R. Bertram, E. Kemnitz, Chem. Mater. 20 (2008) 5687–5697.
[16] G. Tavčar, T. Skapin, unpublished results.
[17] S. Wuttke, S.M. Coman, G. Scholz, H. Kirmse, A. Vimont, M. Daturi, S.L.M. Schroeder, E. Kemnitz, Chem. Eur. J. 14 (2008) 11488–11499.
[18] M. Wojciechowska, A. Wajnert, I. Tomska-Foralewska, M. Zielinski, B. Czajka, Catal. Lett. 128 (2009) 77–82.
[19] K.O. Christe, D.A. Dixon, D. McLemore, W.W. Wilson, J.A. Sheehy, J.A. Boatz, J. Fluorine Chem. 101 (2000) 151–153.
[20] E.K.L.Y. Hajime, J.L. Delattre, A.M. Stacy, Chem. Mater. 19 (2007) 894–902.
[21] J. Slivnik, J. Maček, A. Rahten, B. Sedej, Thermochim. Acta 39 (1980) 21–33.
[22] A. Rahten, P. Benkič, A. Jesih, Acta Chim. Slov. 46 (1999) 339–354.
[23] S.V. Kuznetsov, V.V. Osiko, E.A. Tkatchenko, P.P. Fedorov, Russ. Chem. Rev. 75 (2006) 1065–1082.
[24] S. Javorič, G. Dražič, M. Kosec, J. Eur. Ceram. Soc. 21 (2001) 1543–1546.
[25] P.A. Stadelmann, Ultramicroscopy 21 (1987) 131–145.
[26] S. Chaudhuri, P. Chupas, B.J. Morgan, P.A. Madden, C.P. Grey, Phys. Chem. Chem. Phys. 8 (2006) 5045–5055.
[27] C.L. Bailey, S. Mukhopadhyay, A. Wander, B.G. Searle, N.M. Harrison, J. Phys. Chem. C 113 (2009) 4976–4983.
[28] C.L. Bailey, A. Wander, S. Mukhopadhyay, B.G. Searle, N.M. Harrison, J. Chem. Phys. 128 (2008) 224703–224708.
[29] A. Wander, C.L. Bailey, S. Mukhopadhyay, B.G. Searle, N.M. Harrison, J. Phys. Chem. C 112 (2008) 6515–6519.